Double Quantum ^{1}H MAS NMR Studies of Hydrogen-Bonded Protons and Water Dynamics in Materials

Todd M. Alam,*,† May Nyman,‡ and Sarah K. McIntyre†

Department of Nanostructured and Electronic Materials and Department of Geochemistry, Sandia National Laboratories, Albuquerque, New Mexico 87185

Received: September 20, 2006; In Final Form: January 2, 2007

Two-dimensional double quantum (DQ) ^{1}H MAS NMR was used to investigate different proton environments in a series of alkali (Na, K, Rb, Cs) $[Nb_6O_{19}]^{8-}$ Lindqvist salts, with the water and hydrogen-bound intercluster protons being clearly resolved. Through the analysis of the DQ ^{1}H NMR spinning sideband pattern, it is possible to extract both the mean and distribution of the motionally averaged intramolecular homonuclear ^{1}H−^{1}H dipolar coupling for the different water environments and the intercluster protons. Motional order parameters for the water environments were then calculated from the averaged dipolar couplings. The influence of additional intermolecular dipolar couplings due to multispin interactions were simulated and discussed.

Introduction

Water plays an important role in both the structure and properties of materials,[1−4] including the continued interest in confinement effects within small pores or at interfaces.[5−9] Therefore, a variety of experimental techniques, including neutron scattering,[7,10−12] dielectric spectroscopy,[13] surface force balance measurements,[6] and NMR spectroscopy,[7,10,14−16] have been used to probe the structural and dynamical properties of water in materials. The most common NMR method for studying water dynamics in materials has been line shape and relaxation studies involving static ^{2}H NMR.[17−24] These ^{2}H studies require synthesis of materials with D_2O or the exchange of existing waters, with both approaches almost never being trivial. Chemical shift resolution of different water environments is commonly difficult because of the wide ^{2}H spectral line shape, but different motional environments are often distinguished. Static ^{1}H NMR studies have also been reported[25−30] but again are often limited in the ability to resolve different water species. Magic angle spinning (MAS) ^{1}H, ^{2}H, and ^{17}O NMR investigations of water are also possible and allow different chemical shift environments to be resolved.[18,31−36] In the case of ^{1}H MAS NMR, the spinning speed needs to be faster than the residual ^{1}H−^{1}H dipolar line width for complete chemical shift resolution,[37,38] which for dynamically restricted water molecules is on the order of 40 kHz.

In this paper, the dynamics of water environments in a series of polyoxoniobate alkali salts is investigated using 2D double quantum (DQ) ^{1}H MAS NMR. This method combines the chemical shift resolution afforded by high-speed MAS, with the ability to measure residual dipolar couplings and corresponding water order parameters by analysis of the DQ line shape, without the need to utilize isotopic substitution.

Experimental Section

The synthesis of $Na_7[HNb_6O_{19}]\cdot 15H_2O$ (**I**), $K_7[HNb_6O_{19}]\cdot 10H_2O$ (**II**), $Rb_6(H_3O)_2[Nb_6O_{19}]\cdot 17H_2O$ (**III**), and $Cs_6[H_2Nb_6O_{19}]\cdot 9H_2O$ (**IV**) is given in the Supporting Information and has been described in detail previously.[39] The solid-state ^{1}H MAS NMR spectra were obtained on a Bruker Avance 600 operating at 600.14 MHz, using a 2.5 mm broadband probe at spinning speeds (ν_R) between 30 and 33 kHz. The ^{1}H chemical shifts were referenced to the solid external secondary sample adamantane ($\delta = +1.63$ ppm with respect to TMS $\delta = 0.0$ ppm). It is known that for spinning speeds >25 kHz significant frictional heating occurs. The actual sample temperature was calibrated using the ^{207}Pb chemical shift change of a secondary $Pb(NO_3)_2$ sample.[40,41] All temperatures reported are the corrected sample temperature based on this calibration. The 2D DQ ^{1}H MAS spinning sideband experiments utilized the chemical shift anisotropy (CSA) and off-set compensated back-to-back (BABA) multiple pulse sequence for the excitation and reconversion of the multiple quantum coherences as shown in Figure 1a.[42] For the DQ sideband experiments, the $0 \rightarrow \pm 2 \rightarrow 0 \rightarrow 1$ coherence pathway was selected using a 64-step phase cycle, 200−400 nonrotor synchronized t_1 increments, a 3 μs $\pi/2$ pulse length, and 8−64 scan averages. Typical conditions include a spectral width of 500 kHz ($N = 2$) or 1 MHz ($N = 4$) for the F_1 dimension and 60 kHz for the F_2 dimension, where N is the number of rotor periods. Phase-sensitive detection in the F_1 dimension was obtained using the States-TPPI method.[43] The excitation/reconversion lengths used to obtain the DQ sidebands are dependent on the spinning speed used but for $\nu_R = 33$ kHz, $\tau_{exe} = 60.6$ μs ($N = 2$), and 121.2 μs ($N = 4$). The DQ sideband patterns were obtained by taking the F_1 slice along the ^{1}H chemical shift of interest. These F_1 slices were analyzed for determination of the effective dipolar coupling. The 2D dipolar filtered DQ ^{1}H MAS NMR spinning sideband experiment was performed by inserting a 12-pulse dipolar filter immediately in front of the standard DQ experiment as shown in Figure 1b. This dipolar filter selects the DQ sidebands of those ^{1}H populations that have longer T_2 values (are more mobile). The phase cycling and timing of the dipolar filter experiment has been detailed elsewhere.[44]

Theoretical Methods. The dipolar coupling (D^{ij}) between protons i and j separated by a distance r_{ij} is given by

* Corresponding author. Fax: +505 844-2974; e-mail:tmalam@sandia.gov.
† Department of Nanostructured and Electronic Materials.
‡ Department of Geochemistry.

10.1021/jp066172l CCC: $37.00
Published on Web 02/15/2007

$$D_{ij} = \frac{\mu_0 \hbar \gamma_i \gamma_j}{4\pi\, r_{ij}^3} \quad (1)$$

where μ_0 is the vacuum permeability and $\gamma_{i,j}$ are the magnetic ratios of the interacting protons. For an isolated spin-1/2 pair, the signal intensity of the DQ sidebands (I_{DQ}) is described by[42,45]

$$I_{DQ}(t_1;t_2 = 0) = \cos(2\Delta\omega_{PC}t_1)\left\langle \sin\left[\frac{3}{\pi\sqrt{2}} D_{eff}^{ij} \sin(2\beta^{ij}) \cos(\gamma^{ij} + \omega_R t_1) N\tau_R\right] \times \sin\left[\frac{3}{\pi\sqrt{2}} D_{eff}^{ij} \sin(2\beta^{ij}) \cos(\gamma^{ij}) N\tau_R\right]\right\rangle \quad (2)$$

where D_{eff}^{ij} is the effective dipolar coupling between protons i and j, $\Delta\omega_{PC}$ is the frequency increment for States-TPPI, t_1 is the DQ evolution time increment, $\omega_R (= 2\pi\nu_R)$ is the spinning frequency, N is the number of rotor periods in the excitation/reconversion portion of the BABA sequence, $\tau_R (= \nu_R^{-1})$ is the rotor period, β^{ij} and γ^{ij} are the Euler angles describing the orientation of the principal axis of the dipolar coupling tensor between spins i and j within the reference frame fixed to the rotor, and the symbol $\langle\ \rangle$ represents the Euler angle powder average. If a distribution of effective dipolar couplings is present, then the observed DQ signal intensity can be described by[46]

$$I_{DQ}(t_1,\rho_l) = \sum_l \rho_l \cos(2\Delta\omega_{PC}t_1) \times \left\langle \sin\left[\frac{3}{\pi\sqrt{2}} D_{eff}^{ij}(l) \sin(2\beta^{ij}) \cos(\gamma^{ij} + \omega_R t_1) N\tau_R\right] \times \sin\left[\frac{3}{\pi\sqrt{2}} D_{eff}^{ij}(l) \sin(2\beta^{ij}) \cos(\gamma^{ij}) N\tau_R\right]\right\rangle \quad (3)$$

where ρ_l is the probability of a given effective dipolar coupling $D_{eff}^{ij}(l)$. We have made the simplifying assumption that no correlations exist between $D_{eff}^{ij}(l)$ and the Euler angles β^{ij},γ^{ij}. For the analysis in this paper, a Gaussian probability distribution of the effective dipolar couplings is assumed with mean effective dipolar coupling, $\bar{D}_{eff}^{ij}$, and a standard deviation, σ, defined by

$$\rho_l(D_{eff}^{ij}, \sigma) = \frac{1}{\sqrt{2\pi}} \exp\left[-\frac{1}{2}\left(\frac{\bar{D}_{eff}^{ij} - D_{eff}^{ij}(l)}{\sigma}\right)^2\right] \quad (4)$$

The distribution width, σ, used in eq 4 utilizes a more standard Gaussian distribution definition and differs from that reported previously in ref 49. The full width at half-maximum of the distribution is given by $2\sqrt{2\ln 2}\sigma \approx 2.35\sigma$, with the σ values differing by a scaling factor of $\sqrt{2}$ from those σ values obtained using the definition in ref 49. Simulation of the DQ sidebands were performed in MATLAB (Mathworks, Inc.) using eqs 3 and 4, with the powder average over β and γ implemented using the Grant tiling scheme.[47]

The multispin DQ ^{1}H MAS NMR spinning sideband patterns were simulated using the SIMPSON program[48] on a eight-node AMD Linux cluster. All simulations used a 30 kHz spinning speed, along with a 3 μs $\pi/2$ pulse length to explicitly evaluate the impact of finite pulse widths on the DQ sideband pattern. The two-spin calculations using SIMPSON resulted in DQ sideband patterns that were nearly identical to those obtained using the analytical solution in eq 2. A series of three-spin, four-spin, and five-spin simulations were performed and are presented in both the discussion section and the Supporting Information. DQ simulation involving six spins or higher proved too time intensive using our present computational resources.

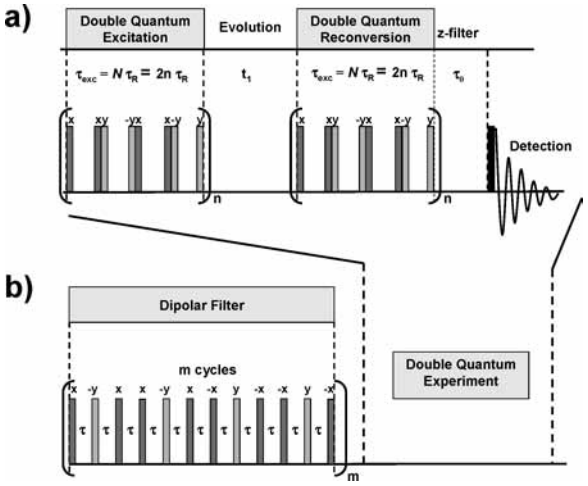

Figure 1. (a) 2D nonrotor synchronized DQ ^{1}H MAS NMR correlation pulse sequence and (b) the dipolar-filtered DQ ^{1}H MAS NMR pulse sequence.

Results

The 1D ^{1}H MAS NMR spectra at 54.5 °C for the Na, K, Rb, and Cs salts (compounds **I**−**IV**) of the $[Nb_6O_{19}]^{8-}$ Lindqvist anion are shown in Figure 2. For **I** (Na compound) two proton signals are observed (Figure 2a): a broad resonance at $\delta = +6.3$ ppm (fwhm = 3160 Hz) and a smaller narrow resonance at $\delta = +1.9$ ppm (fwhm = 700 Hz). Similarly, for **II** (K compound) a broad resonance at $\delta = +6.5$ ppm (fwhm = 2710 Hz) and a smaller narrow resonance at $\delta = +1.5$ ppm (fwhm = 400 Hz) was also observed (Figure 2b). For **III** (Rb compound), two major broad resonances were observed at $\delta = +6.4$ ppm (fwhm = 1720 Hz) and at $\delta = +10.3$ ppm (fwhm = 1430), along with minor resonances at $\delta = +2.0$, +13.3, +14.2, and +16.5 ppm (Figure 2c). For **IV** (Cs compound), broad resonances were observed at $\delta = +5.6$ (fwhm = 1380 Hz) and at $\delta = +8.9$ ppm (fwhm = 715 Hz), along with the narrow minor resonance at $\delta = +1.5$ ppm.

The 2D DQ ^{1}H MAS NMR spectrum for **IV** is shown in Figure 3. On top of the 2D spectra is the single quantum (SQ) projection, and on the right are the individual DQ spectra for different select ^{1}H chemical shifts (shown as dashed vertical color lines in the 2D spectrum). These F_1 dimension DQ NMR spectra clearly show spinning sideband patterns and are used in the analysis of effective dipolar couplings (D_{eff}^{ij}) presented below. Figure 3a (blue) shows the DQ sideband pattern for the $\delta = +8.9$ ppm slice, Figure 3b (red) shows the DQ sideband pattern for the $\delta = +5.6$ ppm slice, and Figure 3c (green) shows the DQ sideband pattern for the $\delta = +1.5$ ppm slice. The odd-numbered spinning sidebands in these DQ spectra are labeled. The * in the DQ sideband spectra denote sidebands arising from adjacent overlapping chemical shifts. This type of 2D DQ ^{1}H MAS NMR spectrum and corresponding DQ sideband patterns are representative of the experimental DQ NMR spectra obtained for compounds **I**−**III** (data not shown).

The experimental (black) and simulated (red) DQ ^{1}H NMR sideband patterns for the different proton resonances in compounds **I** − **IV** are shown in Figure 4. The sideband patterns for the water resonance in the Na (**I**) Lindqvist salt are shown

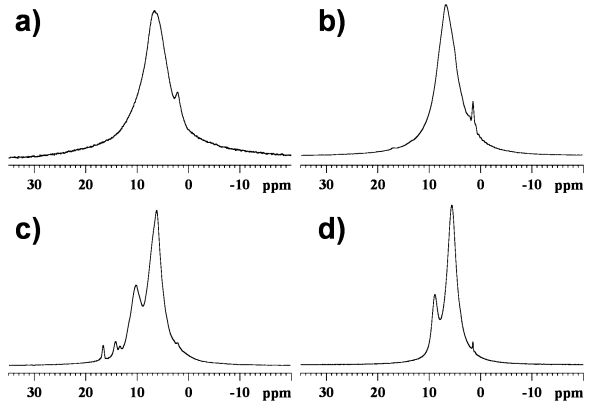

Figure 2. 1D ^{1}H MAS NMR spectra of (a) compound **I** (Na), (b) compound **II** (K), (c) compound **III** (Rb), and (d) compound **IV** (Cs) obtained at spinning speeds (ν_R) between 30 and 33 kHz.

in 4a and b, using $N = 2$ and $N = 4$ rotor cycle excitation/reconversion periods, while 4c ($N = 2$) and 4d ($N = 4$) show the DQ sideband pattern for the water resonance in the K (**II**) salt. The DQ sideband patterns for the Rb compound (**III**) water resonance at $\delta = +6.4$ ppm are shown in 4e ($N = 2$) and 4f ($N = 4$), with the sideband patterns for the water resonance at $\delta = +10.3$ ppm being shown in 4g ($N = 2$) and 4h ($N = 4$). Similarly, the DQ sideband patterns ($N = 2$ and 4) for the $\delta = +5.6$ and $\delta = +8.9$ ppm resonances in the Cs compound (**IV**) are shown in Figure 4i and j, and 4k and l, respectively. For all compounds, the $N = 2$ and $N = 4$ DQ sideband patterns were fit individually with the resulting $\bar{D}^{ij}_{eff}$ and σ shown in Table 1. The D^{ij}_{eff} distributions for the different water environments in **I**−**IV** obtained from these simulations are shown in Figure 5. The variations of these ^{1}H DQ NMR sideband patterns were also investigated for **II** and **IV** over a limited temperature range (5.5−44.6 °C) with no significant change in the sideband pattern or D^{ij}_{eff} distribution observed. The variable-temperature ^{1}H DQ NMR sideband spectra are presented in the Supporting Information (Figure 1S and 2S).

Figure 6 shows the DQ ^{1}H NMR sideband patterns for **II** obtained using the dipolar filtered ^{1}H DQ MAS NMR pulse sequence shown in Figure 1b. With increasing length of the delay (τ) in the dipolar filter, the number and intensity of the higher order DQ sidebands greatly diminish, with the $\tau = 5\ \mu$s filtered DQ spectra showing only significant contribution from the central ± 1 and ± 3 spinning sidebands.

Discussion

The 1D ^{1}H MAS NMR results show that multiple proton environments are present in the different alkali $[Nb_6O_{19}]^{8-}$ Lindqvist salts investigated. A single broad resonance was observed in **I** and **II** with the chemical shift between $\delta = +6.3$ and +6.5 ppm (varies with temperature[49]) and has been assigned to hydrogens belonging to lattice water bonded to the alkali cation and/or H-bonded to the basic oxo-sites on the $[Nb_6O_{19}]^{8-}$ cluster (observed O−H···O bonding generally features a 0.8−0.9 Å O−H distance, and 162−175° O−H···H bond angle).[49] This is consistent with previous ^{1}H NMR studies of niobium oxide where water molecules in rapid exchange with hydroxyl and acid protons were observed between $\delta = +5.1$ and + 6.4 ppm.[50] For **III**, two distinct resonances were observed with a water environment at $\delta = +6.4$ ppm and a second proton environment at $\delta = +10.3$ ppm. This second environment has been assigned to an acidic hydronium (H_3O^+) species bound to the $[Nb_6O_{19}]^{8-}$ cluster. This resonance revealed a moderate DQ signal due to ^{1}H−^{1}H dipolar coupling (see Figure 4g and h, and the nonvanishing $\bar{D}^{ij}_{eff}$ in Table 1), arguing against assignment as an isolated H^+ but instead supporting the assignment of this ^{1}H resonance as resulting from coupled protons present in H_2O or H_3O^+ environments. Assignments of H_3O^+ species at these higher δ values have been reported for other materials.[32] The observation of two distinct resonances for **III** shows that the exchange between these two water environments must be slower than ~2300 Hz.

For **IV**, two distinct resonances were also observed with a water environment at $\delta = +5.6$ ppm and a second proton environment at $\delta = +8.9$ ppm. For this phase, the high chemical shift resonance has been assigned to protons on the bridging oxygen (O_BH) that link the superoctahedral faces of adjacent clusters via hydrogen bonds.[39] It has been demonstrated that there is a linear decrease in the solid-state ^{1}H NMR chemical shift with increasing H···O hydrogen bond length given by[51,52]

$$\delta_{^1H} = 44.68 - 19.3d\text{OH}\cdots\text{O (Å)} \qquad (5)$$

The crystal structure of **IV** shows an average intercluster hydrogen bond length of 1.88 Å, with eq 5 predicting a ^{1}H NMR chemical shift of $\delta = +8.4$ ppm, in excellent agreement with the experimental results. The O_BH resonance also reveals a moderate DQ signal due to intramolecular ^{1}H−^{1}H dipolar coupling of adjacent protons on the octahedral face (see Figure 4k and l, and the nonvanishing $\bar{D}^{ij}_{eff}$ in Table 1). Again, the presence of the DQ signal shows that this proton resonance does not result from an isolated proton. In addition to the water and hydrogen-bound O_BH environments, the ^{1}H MAS NMR of compound **I** also has a signal assigned to an isolated basic NbOH proton ($\delta = +1.9$ ppm),[49] while **II** and **IV** also show small amounts of basic NbOH impurities. In this paper, we will concentrate on the dynamics of the hydrogen-bonded O_BH and water protons and therefore will not discuss the isolated basic NbOH protons further.

DQ Sideband Analysis. The 2D DQ ^{1}H MAS NMR experiments (Figures 3 and 4) show that analysis of the spinning sideband patterns can provide a measure of average effective dipolar coupling ($\bar{D}^{ij}_{eff}$) and distribution width (σ). From these effective dipolar couplings, it is possible to then calculate a water order parameter (S_{H_2O}) using

$$S_{H_2O} = \bar{D}^{ij}_{eff}/D^{ij}_{rigid} \qquad (6)$$

where D^{ij}_{rigid} is the dipolar coupling in a motionally rigid water molecule. For a rigid water molecule with a ^{1}H−^{1}H distance of 1.54 Å, a dipolar coupling ($D^{ij}_{rigid}/2\pi$) of 33.4 kHz is predicted using eq 1.[53] The sensitivity of the DQ ^{1}H NMR sidebands to changes in D^{ij}_{eff} (or equivalently S_{H_2O}) are shown in Figure 7. For large D^{ij}_{eff} (large S_{H_2O}), high-order DQ sidebands up to ± 15 and ± 17 are easily observable. As D^{ij}_{eff} and S_{H_2O} decrease, the higher order DQ sidebands disappear. For example, two dipolar coupled protons with $D^{ij}_{eff}/2\pi = 16.7$ kHz ($S_{H_2O} = 0.5$) only have DQ sidebands out to ± 9 that are readily visible. The DQ sideband patterns also depend on the length of the excitation/reconversion periods via ν_R and N as seen in eq 2 and have been discussed in detail elsewhere.[42,45] Figure 4 shows that the water environments in the polyoxoniobate materials presented here have experimental DQ sidebands out to ± 15, consistent with the rather large measured D^{ij}_{eff} (Table 1).

It is also possible to estimate an order parameter for the hydrogen-bonded O_BH protons in **IV** by determining the ratio between the effective and static dipolar couplings, where the

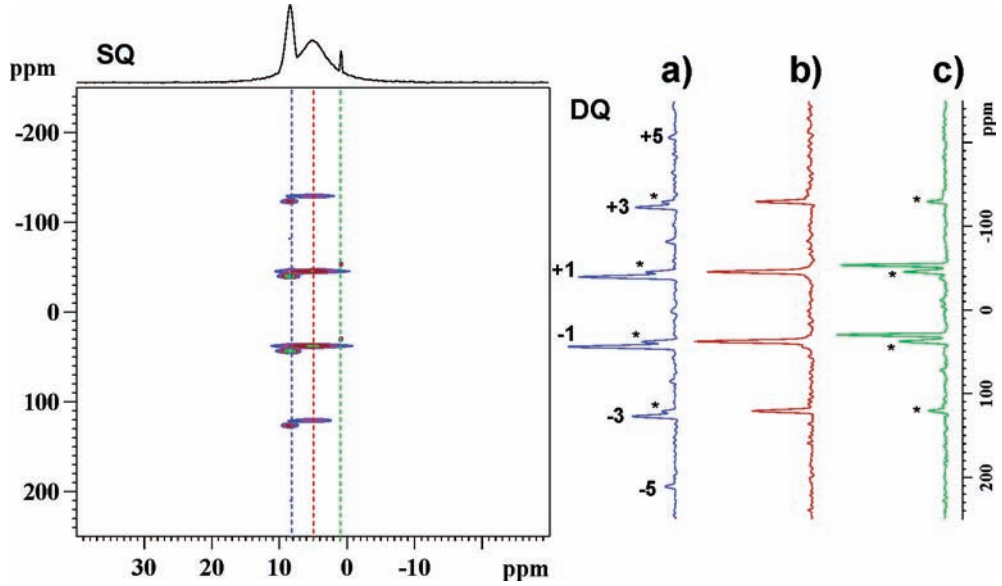

Figure 3. 2D DQ ^{1}H MAS NMR spectrum for compound **IV** using $N = 2$ rotor cycle excitation/recoversion BABA sequence at $\nu_R = 25$ kHz. The top 1D spectrum shows the projection of the single quantum (SQ) F_2 dimension. On the right are 1D spectra for individual double quantum (DQ) F_1 slices at different chemical shifts of interest (dashed color lines): (a) $\delta = +8.9$ ppm, (b) $\delta = +5.6$ ppm, and (c) $\delta = +1.5$ ppm. The odd-numbered sidebands are numbered. The * denotes DQ spinning sidebands resulting from overlapping chemical shifts and are not considered in the analysis.

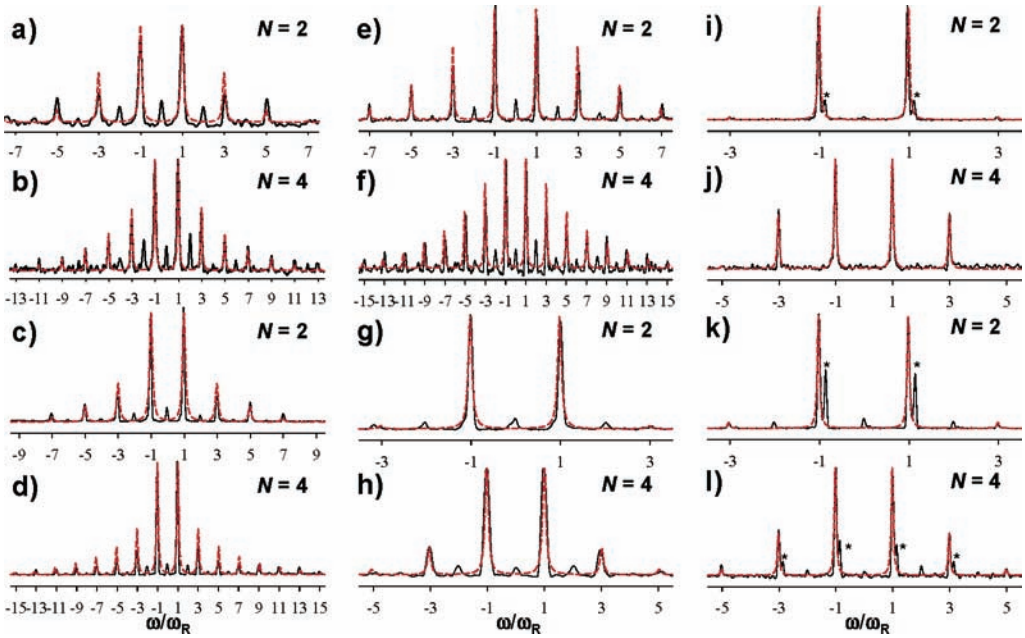

Figure 4. Experimental (black) and simulated (red) DQ ^{1}H MAS NMR sidebands for (a) the $\delta = +6.3$ ppm water resonance in **I**, $N = 2$ rotor cycles and (b) $N = 4$ rotor cycles. (c) The $\delta = +6.5$ ppm water resonance in **II**, $N = 2$ and (d) $N = 4$. (e) The $\delta = +6.4$ ppm water resonance in **III**, $N = 2$ and (f) $N = 4$. (g) The $\delta = +10.3$ ppm hydronium resonance in **III**, $N = 2$ and (h) $N = 4$. (i) The $\delta = +5.6$ water resonance in **IV**, $N = 2$ and (j) $N = 4$. (k) The $\delta = +8.9$ ppm hydrogen-bound proton resonance in **IV**, $N = 2$ and (l) $N = 4$. The * denotes DQ spinning sidebands resulting from overlapping chemical shifts and are not considered in the analysis.

static dipolar coupling is based on the nearest ^{1}H−^{1}H contact present within the material. For example, the intramolecular ^{1}H−^{1}H distance for the O_BH protons in **IV** is 2.55 Å, which would predict a 7.3 kHz dipolar coupling using eq 1. The intermolecular ^{1}H−^{1}H distances for these hydrogen-bonded O_BH protons are 3.13 Å ($D^{ij}_{\text{rigid}}/2\pi = 4$ kHz) and 5.03 Å (0.9 kHz), suggesting that to first order the intramolecular dipolar coupling would be dominant and is consistent with the measured 7.0 and 7.5 kHz effective dipolar coupling (see Table 1). Unfortunately, the crystal structure for this material also reveals a close 2.86 Å ^{1}H−^{1}H contact between the O_BH protons and neighboring waters, which in the static limit would produce a 5.2 kHz dipolar coupling. This additional coupling would produce perturbations on the observed DQ spectra. Alternatively, the significant motions observed for the waters in **IV** ($S_{H_2O} \sim 0.18$, see discussion below) would result in a further reduction in the magnitude of this perturbing coupling. Using these assumptions, the order parameters for the different proton environments in compounds **I**−**IV** are shown in Table 1.

Distribution of Effective Dipolar Couplings and Water Dynamics. Analysis of the experimental DQ sidebands for **I**−**IV** in Figure 4 using a simple two-spin approximation (eq 2) resulted in very poor fits. In particular, the relative ratio of the central ±1 transition intensity to the intensity of higher order

TABLE 1: Effective Dipolar Coupling, Distributions, and Order Parameters Obtained from Simulation of ^{1}H DQ MAS NMR Spinning Sideband Patterns for the Water and Hydrogen-Bound Intermolecular Resonances for Compounds I−IV

water resonance compound	δ (fwhm)[a]	$\bar{D}^{ij}_{eff}/2\pi$ (kHz) ($N=2$)[b]	σ (kHz) ($N=2$)[b]	$\bar{D}^{ij}_{eff}/2\pi$ (kHz) ($N=4$)[b]	σ (kHz) ($N=4$)[b]	$\langle S\rangle$ ($N=2$)	$\langle S\rangle$ ($N=4$)
Na (**I**)	6.3 (3160)	23 ± 1	4.5	24 ± 1	4.5	0.69[c]	0.72[c]
K (**II**)	6.5 (2710)	33 ± 1	12	33 ± 1	10	0.99[c]	0.99[c]
Rb (**III**)	6.4 (1720)	32 ± 1	8	31 ± 1	7	0.96[c]	0.93[c]
	10.3 (1430)	8 ± 1	2	8 ± 1	2	0.24[c]	0.24[c]
Cs (**IV**)	5.6 (1380)	6 ± 1	0.5	6 ± 1	0.5	0.18[c]	0.18[c]
	8.9 (715)	7 ± 1	<0.5[e]	7.5 ± 1	1.5	0.96[d]	~1[d]

[a] Chemical shift = δ (ppm) and line width fwhm = full width at half-maximum (Hz). [b] The effective average dipolar coupling and distribution defined in eqs 2−4 for $N=2$ and $N=4$ rotor cycle DQ excitations/reconversion periods. [c] Effective order parameter for water defined using eq 4, assuming a static ^{1}H−^{1}H dipolar coupling of 33.4 kHz. [d] Effective order parameter for the hydrogen-bonded O_BH protons defined using eq 4, assuming a static ^{1}H−^{1}H dipolar coupling 7.3 kHz (^{1}H−^{1}H distance 2.55 Å) for Cs (**IV**). [e] Lack of higher order sidebands makes determination of σ difficult.

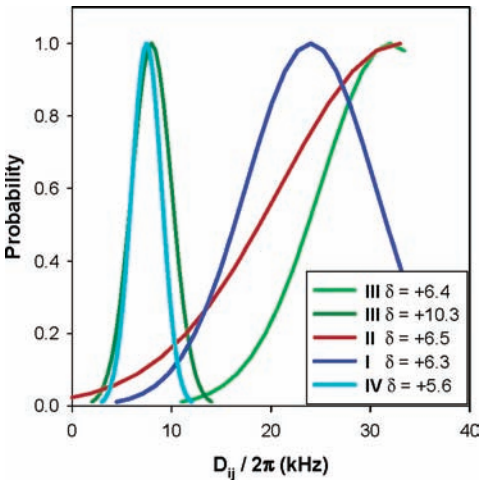

Figure 5. Effective dipolar coupling distributions for the different water species in compounds **I**−**IV** determined by DQ ^{1}H MAS NMR.

sidebands could not be simulated correctly. This discrepancy has been noted before and has been attributed to either multispin effects or distributions in D^{ij}_{eff}.[46,54] A simple model using a distribution of D^{ij}_{eff} (eqs 3 and 4) can simulate the experimental spectra very well at both $N=2$ and $N=4$ rotor cycle excitation/reconversion experiments as shown in Figure 4 and Table 1.

The average $\bar{D}^{ij}_{eff}$ and corresponding distributions for the water (and hydronium) species in compounds **I**−**IV** were different (see Figure 5). The water species ($\delta = +6.4$ and $+6.5$ ppm) in the K and Rb compounds (**II** and **III**) are extremely rigid, with the average order parameter S_{H_2O} greater than ~0.95. Both of these compounds show a large distribution (σ), implying that a range of water dynamics is present within the material. This large distribution is not surprising for these niobium materials considering that for all compounds multiple waters are present within the unit cell. For example, compound **II**, $K_7[HNb_6O_{19}]\cdot 10H_2O$, has 10 distinct waters based on crystallography, whereas **III**, $Rb_6(H_3O)_2[H_2Nb_6O_{19}]\cdot 17H_2O$, has 19 distinct waters on 6 distinct crystallographic sites. These waters are directly associated via hydrogen bonding to the bridging and terminal oxo-sites of the $[Nb_6O_{19}]^{8-}$ clusters, while other lattice water species are more removed and may be coordinated to the counter cations with differing degrees of dynamics. The Na compound (**I**) water species ($\delta = +6.3$ ppm) also has a large $\bar{D}^{ij}_{eff}$ with $S_{H_2O} \sim 0.75$. The distribution for **I** is slightly narrower than that observed for **II** and **III**. These large-order parameters are observed even at the elevated sample temperatures realized in the experiment (between +45 °C and +60 °C), demonstrating that the signal probed during the DQ experiments arises from very immobile water species. Water environments that have a high degree of motional dynamics will have very small effective dipolar couplings and therefore are not excited to the same extent during the DQ pulse sequence. The large line widths associated with the water species in **I** and **II** have been attributed to ^{1}H exchange between different environments,

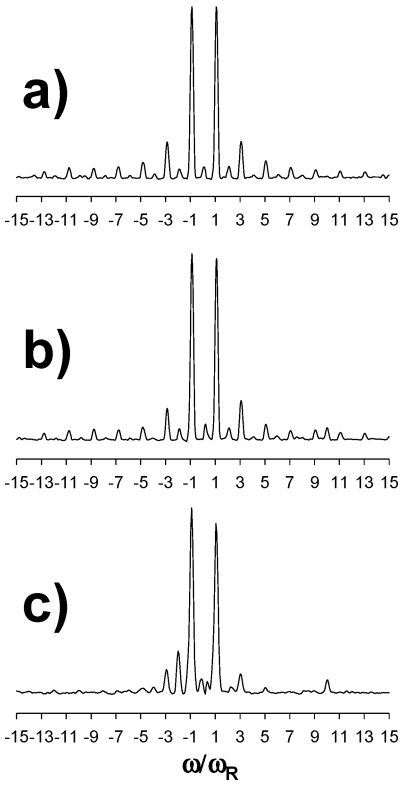

Figure 6. Dipolar-filtered DQ ^{1}H MAS NMR sidebands for the water resonance ($\delta = +6.5$ ppm) compound (**II**) using the pulse sequence in Figure 1b with $N=4$ and $\nu_R = 30$ kHz with (a) no dipolar filter, (b) $\tau = 1$ μs, $m=1$ dipolar filter, and (c) $\tau = 5$ μs, $m=1$ dipolar filter.

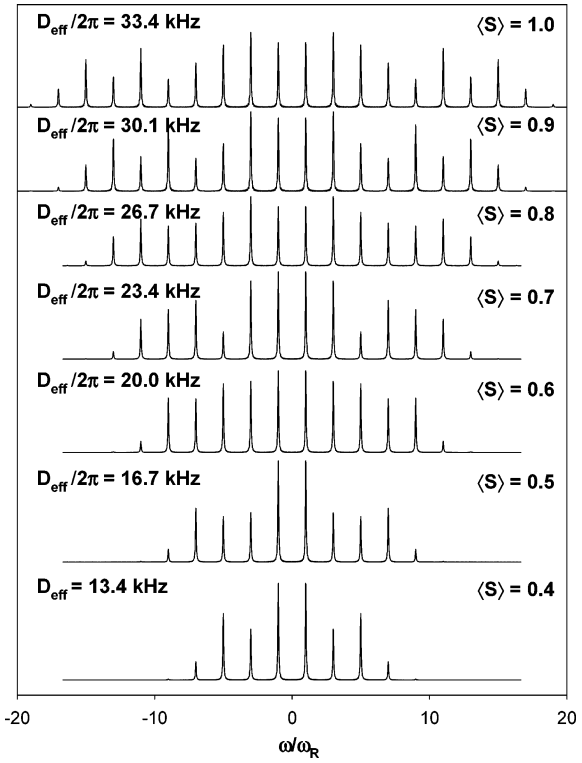

Figure 7. DQ sideband pattern arising from two dipolar coupled spins with different effective dipolar couplings D^{ij}_{eff} and corresponding order parameters S_{H_2O}. Simulations assume $\nu_R = 30$ kHz and $N = 4$.

but it would appear that if this exchange is indeed occurring then it does not average the effective dipolar coupling significantly.

The large S_{H_2O} values experimentally observed limit the type of water dynamics that can occur within these materials. There have been numerous motional models used to describe water dynamics in materials.[28−30,33] Discrete 180° jumps about the $C_{2\nu}$ symmetry axis of the H_2O molecule do not produce an averaging of the ^{1}H−^{1}H dipolar coupling because this motion results in a coincident dipolar tensor. This is in contrast to ^{2}H NMR where the effective ^{2}H quadrupolar coupling is averaged by a discrete two-site jump because the principal component of the quadrupolar electrical field gradient tensor is aligned approximately along the OD bond axis, which changes orientation during the two-site jump process.[24] Alternatively, a continuous spinning motion about the $C_{2\nu}$ axis (axis perpendicular to the ^{1}H−^{1}H dipolar tensor axis) of the H_2O molecule would average the dipolar coupling by $^1/_2$ ($S_{H_2O} = 0.5$) to give a $\bar{D}^{ij}_{\text{eff}}$ of ∼16.7 kHz. The observation of large S_{H_2O} values for **I**−**III** shows that this type of continuous $C_{2\nu}$ spinning motion is not occurring for those water environments. The slight reduction in S_{H_2O} does suggest that there are libration-type motions present (in addition to the possibility of discrete $C_{2\nu}$ flips) leading to the partial averaging of the dipolar coupling.

In contrast, the $\delta = +5.6$ water species of **IV** and the hydronium environment of **III** ($\delta = +10.3$ ppm) show a much smaller dipolar coupling and a corresponding smaller order parameter of $S_{H_2O} = 0.18$ and 0.24, respectively. These water (hydronium) environments are more mobile without a large motional distribution. The motion for these water environments are not an isotropic reorientation because this motion would completely average the dipolar coupling leading to $\bar{D}^{ij}_{\text{eff}} \sim 0$ and $S_{H_2O} \sim 0$. Additional details of the water dynamics responsible for the observed averaging are not possible from the simple analysis of S_{H_2O}.

The Rb (**III**) and Cs compounds (**IV**) highlight one of the advantages of the DQ ^{1}H MAS NMR experiment; motional dynamics can be measured for each chemical shift resolved proton species. In ^{2}H and ^{1}H wide line studies, different ^{1}H environments are typically resolved only if there are differences in dynamics leading to distinguishable line shapes. In **IV**, this is not the situation; these chemically resolved water and hydrogen-bonded O_BH species ($\delta = +5.6$ and 8.9 ppm) have very similar order parameters ($S_{H_2O} = 0.18$ and 0.23, see Table 1) that were directly measured using DQ ^{1}H NMR.

The presence of a distribution of D^{ij}_{eff} is experimentally verified by the dipolar filtered experiments shown in Figure 6. The DQ sideband spectra obtained for **II** with either (a) no dipolar filter or (b) a short 1 μs τ dipolar filter (Figure 6a and b) reveal sidebands out to ±13. When the filter time τ is increased to 5 μs (Figure 6c), the DQ sideband pattern changes dramatically with only the ±1 and ±3 sidebands being observed. This dipolar filter is known to attenuate spin populations that have a short T_2 value (stronger dipolar coupling), whereas spin populations with longer T_2 values (smaller dipolar couplings) receive less attenuation.[44] It has been suggested that the spectral changes observed may result from a subselection of the dipolar orientations from the full powder average (eqs 2 and 3) due to heterogeneous relaxation during the T_2 filter. Simulations of the DQ sideband patterns with different distributions of the Euler angles revealed phase twist in the observed spectra but did not affect the overall relative intensities of the spinning sidebands. These dipolar filtered DQ results therefore demonstrate that the observed DQ sideband patterns are indeed a superposition of different D^{ij}_{eff}, consistent with the distribution model used here.

The temperature dependence of $\bar{D}^{ij}_{\text{eff}}$ and σ was also investigated for select compounds (see Figures 1S and 2S in the Supporting Information). Over a ∼40 °C range (5.5−44.6 °C), there were not significant variations in the observed dipolar coupling for the water in **II** and the $\delta = +8.9$ ppm O_BH resonance in **IV**. These results show that the motional processes of the water environments in these materials have relatively low temperature sensitivity. An interesting observation was that the DQ signal of the water resonance in **IV** was greatly attenuated at the lower temperature (+5.5 °C) in comparison to the higher temperatures (bottom, Figure 2S). In general, lowering the temperature should reduce motional processes that average the dipolar interaction, leading to an increase in D^{ij}_{eff} and the resulting DQ signal. The dramatic loss of DQ intensity suggests that for the water environment in **IV** there were motional processes occurring on the time scale of the BABA pulse sequence.

It is important to note that a Gaussian distribution of D^{ij}_{eff} is not a unique model or description. It is also possible to fit the experimental DQ ^{1}H MAS NMR sidebands with the overlap of individual spectrum for different D^{ij}_{eff}. An example of a bimodal simulation (a mixture of spectra for two discrete D^{ij}_{eff}) of the experimental DQ sideband spectrum for **I** is shown in Figure 3S (Supporting Information). Simulations using the Gaussian distribution model gave smaller residuals in comparison to bimodal model simulations. In addition, the Gaussian model has fewer adjustable parameters. For these reasons, we elected to describe all of the experimental DQ sideband patterns in this paper using a Gaussian distribution of D^{ij}_{eff} (eqs 2−4).

Multispin Effects. For an isolated two-spin dipolar interaction, the resulting DQ sideband pattern is predicted to be composed entirely of odd-ordered spinning sidebands.[42,45] In the experimental DQ sideband spectra for compounds **I**−**IV**, both even- and odd-ordered spinning sidebands were observed

(e.g., Figure 4). Several different explanations have been forwarded to explain these types of even-ordered sidebands. Although many of these possibilities have been discussed previously, it is worthwhile to discuss them briefly. It has been suggested that the appearance of even-ordered sidebands is simply an experimental artifact arising from either pulse or phase imperfections within our instrument. This argument can be dismissed based on simulations along with the experimental results observed in Figure 4 for compound **IV** where the $\delta = +5.6$ ppm water environment shows only odd-ordered sidebands (Figure 4i and j), whereas the $\delta = +8.9$ ppm O_BH proton environment clearly shows even-ordered sidebands (Figure 4k). These results were obtained from the same 2D experiment, arguing against the sidebands simply originating from experimental imperfections. In addition, the similar magnitude of D_{eff}^{ij} for these two different water environments also excludes the appearance of even-ordered sidebands arising from differences in DQ excitation efficiencies for these water resonances. It has also been argued that even-ordered DQ sidebands may also arise from a large ^{1}H chemical shift anisotropy (CSA); an effect that will become more pronounced at higher magnetic field strengths. The impact of the ^{1}H CSA on DQ sideband spectra has been demonstrated previously.[55] In that work, a five-pulse sequence that is sensitive to CSA effects was utilized. In the current investigation, an XY-8 phase cycling of the BABA recoupling sequence was used, which is known to compensate for resonance offsets and CSA to zero order.[42] This insensitivity of the DQ spinning sideband patterns to CSA effects was confirmed through numerical simulations (Figure 4S, Supporting Information) in which very minor changes in the DQ sideband pattern occur for $\Delta\sigma$ values as large as 10 kHz. More importantly, the introduction of a CSA interaction did not lead to the appearance of even-ordered sidebands and therefore is not the cause for the even-ordered sidebands in the experimental spectrum.

Multispin dipolar interactions can give rise to even-ordered sidebands through an evolution rotor modulation mechanism (ERM).[42] Multispin dipolar interactions have also been used to explain the emphasis of the central ± 1 transition of the ^{1}H DQ sideband intensity in PDMS.[54] We had previously argued that multispin effects would have a small impact on the determination of D_{eff}^{ij} based on the degree of perturbation parameter (ξ) forwarded by Schnell and Spiess[42]

$$\xi = \frac{D^{\text{pert}}}{\omega_R} \tag{7}$$

where D^{pert} is the dipolar coupling strength (in angular frequency) of the perturbing spin and ω_R is the angular MAS spinning frequency. Assuming a simple hydrogen-bonded network of water, the closest third spin would be at $\sim$2.2 Å and would produce a perturbation parameter of $\xi < 0.4$ for $\nu_R = 30$ kHz. If there are additional water dynamics occurring, then the perturbing dipolar coupling would be further reduced leading to smaller values of ξ. For small perturbations, it has been argued that accurate dipolar couplings could still be obtained from the analysis of ^{1}H DQ sidebands using a simple two-spin approximation (eq 2).[42]

This issue of multispin interactions was revisited by performing a series of simulations for three-spin, four-spin, and five-spin dipolar coupled ^{1}H clusters to address the changes in the DQ sideband pattern and the introduction of even-ordered sidebands. For the four-spin and five-spin models, there are numerous intermolecular dipolar couplings, such that the degree of perturbation ξ can still be quantified using eq 7 by defining an effective perturbing dipolar coupling via

$$D^{\text{pert}} = \sqrt{\sum_{j>2}^{N} (D_{\text{eff}}^{1j})^2} \tag{8}$$

The results of these multispin DQ sideband simulations are presented in Figures 5S, 6S, and 7S of the Supporting Information. In summary, for $\xi < 0.2$ there are no significant changes in the odd-ordered DQ sideband ratios, even in the presence of multispin interactions. The extraction of meaningful effective dipolar couplings in water molecules can be realized for these smaller perturbations. The $\xi = 0.2$ value is much smaller than our original argument of $\xi = 0.5$ [49] and is something that needs to be considered when trying to extract effective dipolar couplings. Increasing the spinning speeds ($\nu_R \gg 30$ kHz) will decrease ξ (see eq 7) and allow the accurate evaluation of effective intramolecular couplings in water in the presence of larger perturbing intermolecular dipolar couplings. For $\xi > 0.2$, the details of the line shape effects appear to be dependent on the orientation of the intermolecular coupled water species. Multispin interactions are responsible for the even-ordered sidebands and can produce some relative attenuation of the outer sidebands at increased ξ values (>0.15), but these effects do not appear to be large enough to explain the dramatic emphasis of the ± 1 and ± 3 sidebands observed experimentally. For this reason, we will continue to argue the experimental DQ sideband patterns observed arise from a distribution of D_{eff}^{ij}.

These simulations also re-emphasize the inability of DQ ^{1}H MAS NMR sideband analysis to extract extensive structural details or to distinguish between complex motional models. Consider, for example, the models forwarded to describe water dynamics in ^{2}H NMR studies of the molecular sieve VPI-5 [17,18] or the models used for analysis of ^{1}H wide line NMR studies of loading in zeolites.[29,30] Calculating the complete ^{1}H DQ NMR sideband pattern for these types of multisite models would involve an extensive number of parameters, not only the proton−proton exchange rates but also the effective dipolar couplings (averaged distances), distributions of dipolar couplings, and the relative angles of the numerous dipolar interactions. These extensive models are beyond our current computational capabilities and would be poorly constrained given the limited experimental restraints in the DQ sideband data. Alternatively, the ^{1}H DQ NMR experiments provide a simple and quick method of probing materials for variations in water dynamics.

Correlation with Material Properties. Water dynamics have been forwarded previously to explain some of the behavior in polyoxometalates. For example, differences in water dynamics can explain changes in catalytic cyclopropane isomerization on the heteropoly acid $H_3PW_{12}O_{40}$ with increasing amounts of water adsorption.[36] In the present study, the water environment mobility can be ranked as **IV** ($\delta = +5.6$ ppm) $\sim$ **III** ($\delta = +10.3$ ppm) $\gg$ **I** ($\delta = +6.3$ ppm) $>$ **II** ($\delta = +6.5$ ppm) $\sim$ **III** ($\delta = +6.4$ ppm). This ranking of water dynamics differs from the order of average number of alkali−oxygen (cluster) bonds per alkali observed in the structural data,[39] 4.5 (**IV**), 4.33 (**III**), 3.0 (**II**), and 2.0 (**I**), and from the measured degree of solubility, **IV** > **III** > **II** > **I**. It may be possible that the unique hydrogen-bonded cluster structural motif in **IV** and the presence of hydronium water species in **III** may influence the observed solubility and hydroxy species formation. The ranking order of water dynamics also differs from the relative order of measured oxygen exchange rates for the bridging and terminal oxygen sites in solution reported previously, **III** > **IV** > **II**.[39]

Unfortunately, it does not appear that the water dynamics measured for the alkali $[Nb_6O_{19}]^{8-}$ Lindqvist salts using DQ ^{1}H NMR correlate with any of these reported material properties.

Conclusions

We have demonstrated that it is possible to measure the dynamics for chemically distinct proton environments in materials using DQ ^{1}H MAS NMR techniques. The analysis of the DQ sideband patterns provides a direct measure of the effective ^{1}H−^{1}H dipolar coupling for both the water and hydrogen-bonded O_BH proton environments. From this measurement of the dipolar coupling, the motional order parameter of the different proton environments can be calculated. These DQ NMR techniques were used to measure the effective dipolar coupling distributions for a series of alkali $[Nb_6O_{19}]^{8-}$ Lindqvist salts. There are significant differences in the water mobility based on the alkali phase investigated. The water environment in the Cs hexaniobate salt and the hydronium environment in the Rb hexaniobate salt showed the highest degree of water mobility, whereas the water environments of the K and Rb hexaniobates were observed to be extremely immobile. These water mobility rates do not appear to correlate with other material properties such as solubility, oxygen exchange rates, or the average alkali−oxygen bond numbers. These DQ ^{1}H MAS NMR studies provide fundamental insight into the chemical differences and variation in local water dynamics within materials without requiring isotopic substitution.

Acknowledgment. Sandia is a multiprogram laboratory operated by Sandia Corporation, a Lockheed Martin Company, for the United States Department of Energy's National Nuclear Security Administration under Contract DE-AC04-94AL85000. This work was supported under the Sandia LDRD program.

Supporting Information Available: Synthetic details, experimental variable temperature DQ spinning sideband NMR spectra, and simulated DQ sideband spectra for bimodal model, CSA effects, and details for 3, 4, and 5 multispin DQ simulations. This material is available free of charge via the Internet at http://pubs.acs.org.

References and Notes

(1) *Physicochemistry of Thin Film Water in Geological and Biological Systems*; Nakashima, S.; Spiers, C. J.; Mercury, L.; Fenter, P. A.; Hochella, M. F., Eds.; Universal Academy Press: Tokyo, 2004; Vol. 44, p 1.
(2) Vollrath, F.; Porter, D. *Soft Matter* **2006**, *2*, 377.
(3) Taylor, H. F. W. *Cement Chemistry*, 2nd ed.; Thomas Telford Publishing: London, 1997.
(4) Phair, J. W.; Badwal, S. P. S. *Ionics* **2006**, *12*, 103.
(5) Christenson, H. K. *J. Phys.: Condens. Matter* **2001**, *13*, R95.
(6) Klein, J.; Raviv, U.; Perkin, S.; Kampf, N.; Chai, L.; Giasson, S. *J. Phys.: Condens. Matter* **2004**, *16*, S5437.
(7) Chen, S.-H.; Mallamace, F.; Mou, C.-Y.; Broccio, M.; Corsaro, C.; Faraone, A.; Liu, L. *PNAS* **2006**, *103*, 12974.
(8) Levinger, N. E. *Science* **2002**, *298*, 1722.
(9) Zangi, R. *J. Phys.: Condens. Matter* **2004**, *16*, S5371.
(10) Webber, B.; Dore, J. *J. Phys: Condens. Matter* **2004**, *16*, S5449.
(11) Neumann, D. A. *Mater. Today* **2006**, *9*, 34.
(12) Crupi, V.; Dianoux, A. J.; Majolino, D.; Migliardo, P.; Venuti, V. *Phys. Chem. Chem. Phys.* **2002**, *4*, 2768.
(13) Spanoudaki, A.; Albela, B.; Bonneviot, L.; Peyrard, M. *Eur. Phys. J. E* **2005**, *17*, 21.
(14) Veith, S. R.; Hughes, E.; Vuataz, G.; Prantsinis, S. E. *J. Colloid. Interface Sci.* **2004**, *274*, 216.
(15) Turov, V. V.; Leboda, R. *Adv. Colloid Interface Sci.* **1999**, *79*, 173.
(16) Koller, H.; Englehardt, G.; van Santen, R. A. *Top. Catal.* **1999**, *9*, 163.
(17) Goldfarb, D.; Li, H.-X.; Davis, M. E. *J. Am. Chem. Soc.* **1992**, *114*, 3690.
(18) Duer, M.; He, H.; Kolodziejski, W.; Klinowski, J. *J. Phys. Chem.* **1994**, *98*, 1198.
(19) Di Benedetto, S.; Chidichimo, G.; Golemme, A.; Imbardelli, D. *J. Phys. Chem.* **1996**, *100*, 8079.
(20) Chidichimo, G.; Golemme, A.; Imbardelli, D.; Santoro, E. *J. Phys. Chem.* **1990**, *94*, 6826.
(21) Stepanov, A. G.; Shegai, T. O.; Luzgin, M. V.; Essayem, N.; Jobic, H. *J. Phys. Chem.* **2003**, *107*, 12438.
(22) Mizuno, M.; Hamada, Y.; Kitahara, T.; Suhara, M. *J. Phys. Chem. A* **1999**, *103*, 4981.
(23) Wingen, A.; Basler, W.; Lechert, H. Anisotropic Motion of Water in Zeolites EMT, L, and ZSM-5 as Studied by D- and H-NMR Line Splitting. In *Progress in Zeolite and Microporous Materials*; Chon, H., Ihm, S.-K., Uh, Y. S., Eds.; Elsevier Science B. V.: New York, 1997; Vol. 105, p 495.
(24) Kobe, J. M.; Gluszak, T. J.; Dumesic, J. A.; Root, T. W. *J. Phys. Chem.* **1995**, *99*, 5485.
(25) Arun, N. S. V.; Ramanathan, K. V. *J. Phys. Chem. B* **2000**, *104*, 9091.
(26) Wang, P. S.; Ferguson, M. M.; Eng, G.; Bentz, D. P.; Ferraris, C. F.; Clifton, J. R. *J. Mater. Sci.* **1998**, *33*, 3065.
(27) Marcelin, G.; Stockhausen, N. J.; Post, J. F. M.; Schutz, A. *J. Phys. Chem.* **1989**, *93*, 4646.
(28) Tritt-Goc, J.; Pislewski, N. *Mol. Phys.* **1994**, *83*, 949.
(29) Batamack, P.; Dorémieux-Morin, C.; Vincent, R.; Fraissard, J. *Chem. Phys. Lett.* **1991**, *180*, 545.
(30) Batamack, P.; Dorémieux-Morin, C.; Vincent, R.; Fraissard, J. *J. Phys. Chem.* **1993**, *97*, 9779.
(31) Hayashi, S. *J. Mater. Chem.* **1997**, *7*, 1043.
(32) Jeanneau, E.; Le Floch, M.; Bureau, B.; Audebrand, N.; Louër, D. *J. Phys. Chem. Solids* **2004**, *65*, 1213.
(33) Udea, T.; Nakamura, N. *J. Phys. Chem. B* **2003**, *107*, 13681.
(34) Dickinson, L. M.; Harris, R. K.; Shaw, J. A.; Chinn, M.; Norman, P. R. *Magn. Reson. Chem.* **2000**, *38*, 918.
(35) Grünberg, B.; Emmler, T.; Gedat, E.; Shenderovich, I.; Findenegg, G.; Limbach, H.-H.; Buntkowsky, G. *Chem.—Eur. J.* **2004**, *10*, 5689.
(36) Baba, T.; Ono, Y. *Appl. Catal., A* **1999**, *181*, 227.
(37) Schnell, I. *Prog. Nucl. Magn. Reson.* **2004**, *45*, 145.
(38) Samoson, A.; Tuherm, T.; Gan, Z. *Solid State Nucl. Magn. Reson.* **2001**, *20*, 130.
(39) Nyman, M.; Alam, T. M.; Bonhomme, F.; Rodriguez, M. A.; Frazer, C. S.; Welk, M. E. *J. Cluster Sci.* **2006**.
(40) Bielecki, A.; Burum, D. P. *J. Magn. Reson., Ser. A* **1995**, *116*, 215.
(41) Takahashi, T.; Kawashima, H.; Sugisawa, H.; Baba, T. *Solid State Nucl. Magn. Reson.* **1999**, *15*, 119.
(42) Schnell, I.; Spiess, H. W. *J. Magn. Reson.* **2001**, *151*, 153.
(43) Marion, D.; Ikura, M.; Tschudin, R.; Bax, A. *J. Magn. Reson.* **1989**, *85*, 393.
(44) Egger, N.; Schmidt-Rohr, K.; Blumich, B.; Domke, W. D.; Stapp, B. *J. Appl. Polym. Sci.* **1992**, *44*, 289.
(45) Graf, R.; Demco, D. E.; Gottwald, J.; Hafner, S.; Spiess, H. W. *J. Chem. Phys.* **1997**, *106*, 885.
(46) Holland, G. P.; Cherry, B. R.; Alam, T. M. *J. Magn. Reson.* **2004**, *167*, 161.
(47) Sethi, N. K.; Alderman, D. W.; Grant, D. M. *Mol. Phys.* **1990**, *71*, 217.
(48) Bak, M.; Rasmussen, J. T.; Nielsen, N. C. *J. Magn. Reson.* **2000**, *147*, 296.
(49) Alam, T. M.; Nyman, M.; Cherry, B. R.; Segall, J. M.; Lybarger, L. E. *J. Am. Chem. Soc.* **2004**, *126*, 5610.
(50) Batamack, P.; Vincent, R.; Fraissard, J. *J. Catal. Lett.* **1996**, *36*, 81.
(51) Jeffrey, G. A.; Yeon, Y. *Acta. Crystallogr.* **1986**, *B42*, 410.
(52) Alam, T. M.; Fan, H. *Macromol. Chem. Phys.* **2003**, *204*, 2023.
(53) Abragam, A. *Principles of Nuclear Magnetism*; Clarendon Press: Oxford, 1961.
(54) Saalwächter, K. *Chem. Phys. Lett.* **2002**, *362*, 331.
(55) Tekely, P.; Demco, D. E.; Canet, D.; Malveau, C. *Chem. Phys. Lett.* **1999**, *309*, 101.